RADIATION INDUCED ELECTRICAL CURRENT AND VOLTAGE IN DIELECTRIC STRUCTURES

A. R. Frederickson

Air Force Cambridge Research Laboratories

Prepared for:

Defense Nuclear Agency

22 November 1974

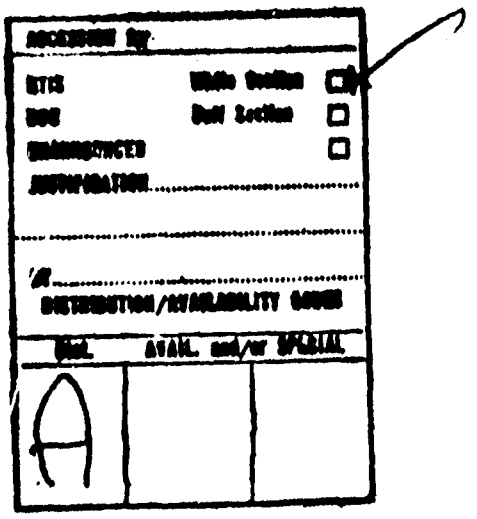

Qualified requestors may obtain additional copies from the Defense Documentation Center. All others should apply to the National Technical Information Service.

Unclassified

SECURITY CLASSIFICATION OF THIS PAGE (When Data Entered)

REPORT DOCUMENTATION PAGE		READ INSTRUCTIONS BEFORE COMPLETING FORM
1. REPORT NUMBER AFCRL-TR-74-0582	2. GOVT ACCESSION NO.	3. RECIPIENT'S CATALOG NUMBER AD-A007 670
4. TITLE (and Subtitle) RADIATION INDUCED ELECTRICAL CURRENT AND VOLTAGE IN DIELECTRIC STRUCTURES		5. TYPE OF REPORT & PERIOD COVERED Scientific. Interim. 6. PERFORMING ORG. REPORT NUMBER PSRP No. 613
7. AUTHOR(s) A. R. Frederickson		8. CONTRACT OR GRANT NUMBER(s)
9. PERFORMING ORGANIZATION NAME AND ADDRESS Air Force Cambridge Research Laboratories (LQ) Hanscom AFB Massachusetts 01731		10. PROGRAM ELEMENT, PROJECT, TASK AREA & WORK UNIT NUMBERS PE 62704H, Work Unit 41 Subtask Z99QAXTA040 Related IHWU CDNA0008
11. CONTROLLING OFFICE NAME AND ADDRESS Air Force Cambridge Research Laboratories (LQ) Hanscom AFB Massachusetts 01731		12. REPORT DATE 22 November 1974 13. NUMBER OF PAGES 41
14. MONITORING AGENCY NAME & ADDRESS(if different from Controlling Office)		15. SECURITY CLASS. (of this report) Unclassified 15a. DECLASSIFICATION/DOWNGRADING SCHEDULE

16. DISTRIBUTION STATEMENT (of this Report)

Approved for public release; distribution unlimited.

17. DISTRIBUTION STATEMENT (of the abstract entered in Block 20, if different from Report)

Reproduced by
NATIONAL TECHNICAL
INFORMATION SERVICE
US Department of Commerce
Springfield, VA. 22151

PRICES SUBJECT TO CHANGE

18. SUPPLEMENTARY NOTES

This research was sponsored by the Defense Nuclear Agency under Work Unit 41, Subtask Z99QAXTA040, "Secondary Electron Phenomenology".

19. KEY WORDS (Continue on reverse side if necessary and identify by block number)

Replacement current; Charge injection; Photo injection; Transient conductivity; Photoconductivity; Photocurrent; Compton current; Electron transport; Dielectric charge; Space charge; Radiation induced conductivity

20. ABSTRACT (Continue on reverse side if necessary and identify by block number)

A computational technique has been developed in one dimension for prediction of radiation-induced electrical currents and electrostatic fields in metal-dielectric slab structures. High energy radiation transport effects produce divergent electron currents, time-dependent electrostatic fields, and time-dependent conduction electron currents. These effects are considered and the computational technique predicts electric fields approaching breakdown intensity and time-dependent electrode currents which may even change sign.

DD FORM 1 JAN 73 1473 EDITION OF 1 NOV 65 IS OBSOLETE

Unclassified

SECURITY CLASSIFICATION OF THIS PAGE (When Data Entered)

20. (Cont)

Brief comments on application of the technique to field effect electronic devices are included. Results are given for several metal-dielectric slab combinations under 200 keV and 1.25 MeV photon irradiations.

Summary

The Air Force has a continuing need to determine the response of electronics to weapons, space, and reactor radiations. Many electronic devices consist of a combination of metallic and dielectric elements. The response of metal-dielectric devices to radiation is not well understood. Experimental studies indicate that such device response cannot yet be predicted. Problems exist with transmission lines, MOS-type transistors, capacitors, large-scale integrated circuits, and compton diodes. The device response to radiation has sometimes been unpredictably time dependent. Similar devices do not always respond in similar ways.

A mechanism which may help to explain the above mentioned difficulties is developed here. Studies on high energy electron transport under Air Force Project 5621 and under Defense Nuclear Agency Subtask Z99QAXTA040 and by the AEC have provided data which allows one to discuss this "new" mechanism quantitatively. It is hoped that the mechanism developed in this report can be used to help clear up some of the difficulties in predicting device response.

High energy radiation induces electrical currents (sometimes called replacement currents) in metallic elements when the metallic elements are adjacent to dielectrics. A cause of these currents is known to be the radiation-induced motion of electrons in the dielectrics. The high energy electron transport in the dielectrics usually produces time varying electric fields. These electric fields cause time-dependent "conduction" currents in the dielectric. Thus the currents induced in metallic elements are time dependent. A mathematical model is presented to determine the time-dependent currents and electric fields. Results are illustrated for X-ray radiations.

Preface

The author wishes to acknowledge the following persons for their help on this work: Dr. Jack Weinberg of RDP Inc. wrote the computer program, and Dr. John Bradford and Edward A. Burke provided continuing critical insight.

Contents

Illustrations

Radiation Induced Electrical Current and Voltage in Dielectric Structures

I. INTRODUCTION

The purpose of this work is to theoretically investigate the following effect. High energy radiations produce electron and photo-compton-electron currents in all materials. Electron currents flowing in a dielectric will induce electrical currents on adjacent conductors. Usually, the dielectric currents are divergent and will deposit electrical charge in the dielectric. This charge deposition produces electrical fields and "conduction" currents in the dielectric, and thereby induces further currents on nearby conductors. We develop a calculational model to predict the induced currents to the conductors. The work is limited to a simple "one dimensional" geometry, which can be compared to controlled experiments and which can be understood without advanced mathematical techniques.

The simplest arrangement of dielectrics and conductors which can be analyzed and experimentally controlled, in one dimension, is shown in Figure 1. All work reported here is limited to this geometry. Extension to more complicated geometry or higher order dimensionality results in greatly increased mathematical and experimental complexity. Removal of any of the elements in Figure 1 results in an arrangement which cannot be useful in a real device application.

(Received for publication 21 November 1974)

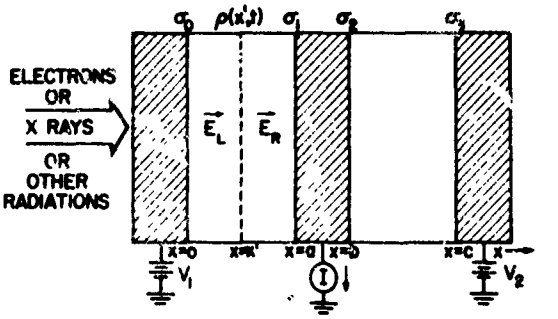

CONDUCTOR
DIELECTRIC
(I) AMPERE METER, Arrow shows positive current direction.
σ is a surface charge density, coulombs/meter^2
ρ is a dielectric charge density, coulombs/meter^3
Radiation travels in the positive X direction.
0,a,b,c are the X positions of the dielectric – metal interfaces
$\vec{E}$ is electric field, volts/meter.

Figure 1. The Simplest Metal Dielectric Structure

2. ELECTROSTATICS

Consider the conditions prior to time t = 0 sec. V_1 and V_2 have been applied and quiescent $\sigma_0(t=0)$, $\sigma_1(t=0)$, $\sigma_2(t=0)$, and $\sigma_3(t=0)$ have been established. No current flows in the meter, I, since the dielectric polarization has equilibrated and since the dielectrics are not "leaky". At $t \geq 0$ sec, we apply the radiation which passes through the material, creating an electron current density $\bar{J}(x, t \geq 0)$ in the $\hat{x}$ direction.

This current density can be described by sheets of charge, $\rho(x,t)dx$ moving with some velocity along the x axis. Every charge sheet is the source of induced electric fields $\bar{E}_L$ and $\bar{E}_R$. The line integral sum equation

$$\int_0^x \bar{E}_L \cdot \bar{dl} + \int_x^a \bar{E}_R \cdot \bar{dl} = 0, \tag{1}$$

is always satisfied. A surface charge density, $\Delta\sigma$, is induced at the conductor surfaces in response to the sheet of charge such that the normal component of the electric field vanishes in the conductor, and we have

$$\bar{E}_L(t) = \frac{+\Delta\sigma_0(t)}{\epsilon}\hat{x} \quad \text{and} \quad \bar{E}_R(t) = \frac{-\Delta\sigma_1(t)}{\epsilon}\hat{x}\,, \tag{2}$$

where $\hat{x}$ is the unit vector and ϵ is the permittivity of the dielectric in F/m. By applying a gaussian surface around the entire system we can show that

$$\Delta\sigma_0(t) + \Delta\sigma_1(t) = -\rho(x,t)dx\,. \tag{3}$$

Combining Eqs. (1), (2), and (3) results in, for $0 \le x \le a$,

$$\Delta\sigma_0(t) = \frac{x-a}{a}\rho(x,t)dx \quad \text{and} \quad \Delta\sigma_1(t) = -\frac{x}{a}\rho(x,t)dx \tag{4}$$

and by a similar process we get, for $b \le x \le c$,

$$\Delta\sigma_2(t) = \frac{x-c}{c-b}\rho(x,t)dx \quad \text{and} \quad \Delta\sigma_3(t) = \frac{b-x}{c-b}\rho(x,t)dx\,. \tag{5}$$

As $\rho(x)$ is distributed over all x, we can sum ρ over all x to obtain the total induced conductor surface charge. For example,

$$\Sigma\Delta\sigma_1(t) = \int_0^a -\frac{x}{a}\rho(x,t)dx$$

$$\sigma_1(t) \equiv \sigma_1(t=0) + \int_0^a -\frac{x}{a}\rho(x,t)dx\,, \tag{6}$$

and similarly,

$$\Sigma\Delta\sigma_2(t) = \int_0^c \frac{x-c}{c-b}\rho(x,t)dx$$

$$\sigma_2(t) \equiv \sigma_2(t=0) + \int_b^c \frac{x-c}{c-b}\rho(x,t)dx\,. \tag{7}$$

3. ELECTRODYNAMICS

The experimentally measurable parameter, I, is composed of the currents required to establish $\sigma_1(t)$ and $\sigma_2(t)$, and the currents actually injected across the metal-dielectric interface. Thus, in our one dimensional case,

$$I(t) = -\frac{d\sigma_1(t)}{dt} - \frac{d\sigma_2(t)}{dt} + J(a,t) - J(b,t) \tag{8}$$

where J is in units of A/m^2.

From Eq. (6) we get

$$\frac{d\sigma_1(t)}{dt} = -\frac{1}{a}\int_0^a x\,\frac{\partial\rho(x,t)}{\partial t}\,dx\,. \tag{9}$$

The continuity equation, $-\frac{\partial\rho}{\partial t} = \bar{\nabla}\cdot\bar{J}$, in the one dimensional geometry of this problem gives

$$\frac{d\sigma_1(t)}{dt} = \frac{1}{a}\int_0^a x\,\frac{\partial J(x,t)}{\partial x}\,dx. \tag{10}$$

Integration by parts results in

$$\frac{d\sigma_1(t)}{dt} = J(a,t) - \frac{1}{a}\int_0^a J(x,t)dx\,, \tag{11}$$

and similarly,

$$\frac{d\sigma_2(t)}{dt} = -J(b,t) + \frac{1}{c-b}\int_b^c J(x,t)dx\,. \tag{12}$$

Substituting into Eq. (8) above, we get

$$I(t) = \frac{1}{a}\int_0^a J(x,t)dx - \frac{1}{c-b}\int_b^c J(x,t)dx. \tag{13}$$

Thus we have shown that the meter current, I(t), depends entirely on the volume integral of current, J(x,t) in the dielectric. In cases where we can establish the current in the dielectric, under radiation, we can predict the meter response. Calculations and measurements of radiation-induced currents are being done elsewhere and will be referenced later in this report. We can assume for the moment, that J(x,t=0) is known.

A new problem arises since we need to know $J(x, t > 0)$. The application of radiation to solids produces conduction electrons (as well as "holes") which can turn a dielectric into a semiconductor. Usually, $J(x, t = 0)$ is such that $\bar{\nabla} \cdot \bar{J} \neq 0$, and charge will be deposited at a rate given by $\frac{\partial \rho(x,t)}{\partial t} = - \bar{\nabla} \cdot \bar{J}(x,t)$. This charge deposition creates a changing electric field in the dielectric, and the radiation-induced conduction electrons move in response to the new electric field strength. Thus, for $t > 0$ we need to include this conduction current in the determination of $J(x, t > 0)$.

We shall calculate this conduction current using the following steps:

(a) Let $n = 0$, where n is a running integer.

(b) Calculate the electric field produced by the charge deposited through a "short" time, Δt.

(c) Determine the conduction current, $J_c(x,t)$, produced by the electric field at the end of the time interval, $t = (n+1)\Delta t$.

(d) Assume that at $t = (n+1)\Delta t$, a new current is flowing defined by $J(x,t) = J(x) + J_c(x,t)$. We will discuss $J_c(x,t)$ and $J(x)$ later.

(e) Step the integer so that $n + 1 = n$ and return to (b) above.

In this way we are able to determine the time dependence of J.

We determine the steps in the following ways.

To calculate the electric field, (b), refer to Figure 2. We calculate E(x) using Gauss' law,

$$\oint \bar{E} \cdot \hat{n} \, dS = \int_V \frac{\rho(v)}{\epsilon} \, dv ,$$

applied to the "gaussian surface". Since the apparatus extends infinitely in the y and z directions, symmetry considerations imply that $\bar{E} \cdot \hat{n}$ must be zero everywhere on the upper and lower sides of the "gaussian surface". $\bar{E} \cdot \hat{n}$ is also zero everywhere in the conductors.

Thus we have

$$\oint \bar{E} \cdot \hat{n} \, dS = AE(x)$$

where A is the cross section area of the "gaussian surface" at x.

At depth x_1 in the dielectric, $\bar{E}$ is produced by charges enclosed in the two gaussian surfaces shown in Figure 2. The total field at x_1 is then given by:

$$E(x_1, t) = \frac{1}{\epsilon} \left[\int_0^{x_1} \rho(x,t)dx - \int_{x_1}^{a} \rho(x,t)dx + \sigma_0(t) - \sigma_1(t) \right] + E_{ext}(x_1) \qquad (14)$$

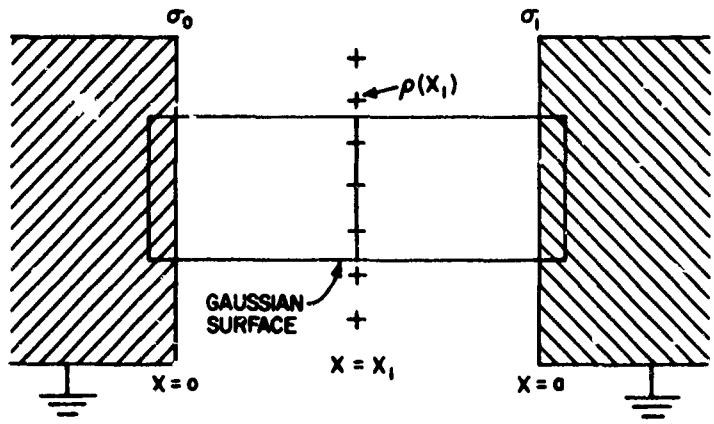

Figure 2. Calculation of Electric Field From Deposited Charge Distribution

where $E_{ext}(x_1)$ is the electric field provided by external voltages as shown in Figure 1. Note that $E_{ext}(x) \equiv E(x, 0)$.

The function $\rho(x, t)$ can be approximately determined from the equation of continuity by

$$\rho(x,t) = \int_{t-\Delta t}^{t} -\bar{\nabla}\cdot\bar{J}(x,t')dt' \cong \rho(x,t-\Delta t) - \Delta t\left[\bar{\nabla}\cdot\bar{J}(x,t-\Delta t)\right]. \tag{15}$$

In this formalism we require that $\bar{J}(x, t')$ not vary significantly (less than 1 percent or so) during the time span $t - \Delta t \leq t' \leq t$. We determine σ_1 [see Eq. (11)] after a short time interval, Δt, by:

$$\sigma_1(t) = \sigma_1(t-\Delta t) + \int_{t-\Delta t}^{t}\left[J(a,t') - \frac{1}{a}\int_0^a J(x,t')dx\right]dt' \tag{16}$$

$$\sigma_1(t) \simeq \sigma_1(t-\Delta t) + \Delta t\left[J(a,t-\Delta t) - \frac{1}{a}\int_0^a J(x,t-\Delta t)dx\right], \tag{17}$$

and similar equations give us σ_0, σ_2, and σ_3 at time t. Thus, for example, the field $E(x_1)$ at time Δt is given by Eqs. (14-17) as

$$\epsilon E(x_1, \Delta t) \cong \epsilon E(x_1, 0) + \int_0^{x_1}\rho(x,0)dx - \Delta t\left[J(x_1,0) - J(0,0)\right] - \int_{x_1}^{a}\rho(x,0)dx + \Delta t\left[J(a,0) - J(x_1,0)\right] + \sigma_0(\Delta t) - \sigma_1(\Delta t) \tag{18}$$

where $E(x_1, 0) \equiv E_{ext}$ evaluated at x_1. We will generally assume that prior to $t = 0$, the dielectrics contain no charge; $\rho(x, 0) = 0$. It is only necessary to know $D(x, 0)$ and $J(x, 0)$ at time $t = 0$ to determine $E(x, \Delta t)$ as long as Δt is sufficiently short.

Now we must determine (c), $J_c(x, t)$. In general, for constant intensity radiation,

$$J(x, t) \equiv J(x) + J_c(x, t) \tag{19}$$

where J_c is a conduction current which is driven by the electric field and $J(x)$ is the field independent radiation-induced high energy electron current. We define

$$J_c(x, t) \equiv \left[\sigma_0 + \sigma_R \dot{D}(x) \right] E(x, t) \tag{20}$$

where $\dot{D}(x)$ is the radiation dose rate in rad/sec, σ_0 is the normal conductivity of the dielectric, and σ_R is the coefficient of radiation-induced conductivity. $\dot{D}(x)$, like $J(x)$, is determined by methods in the literature which will be referenced later. Published experiments indicate that radiation-induced conductivity is proportional to dose rate in many materials.

We are able to determine $I(t = \Delta t)$ from the above equations by evaluating

$$J(x, \Delta t) = J(x) + E(x, \Delta t) \left[\sigma_0 + \sigma_R \dot{D}(x) \right] \tag{21}$$

where $E(x, \Delta t)$ is obtained from Eq. (14) above for $0 < x < a$ and from a similar equation for $b < x < c$, and plugging $J(x, \Delta t)$ into Eq. (13) to get

$$I(\Delta t) = \frac{1}{a} \int_0^a J(x, \Delta t) dx - \frac{1}{c - b} \int_b^c J(x, \Delta t) dx. \tag{22}$$

The cycle (d, e) can now be completed. We have calculated $I(t = 0)$ and $I(t = \Delta t)$. To calculate $I(t = 2\Delta t)$ we have only to go through the calculation again, being careful to replace $t = 0$ by $t = \Delta t$ and also $t = \Delta t$ by $t = 2\Delta t$; and by iterating we can obtain $I(n\Delta t)$ for any reasonable number n.

A computer program has been written to do this calculation by the iterative technique given above. Thus we can determine $I(t)$, $J(x, t)$, $E(x, t)$ for any type of radiation which produces a known $J(x, 0)$ and $\dot{D}(x, 0)$ in this one dimensional geometry.

A flow chart for the computer program is given in Figure 3.

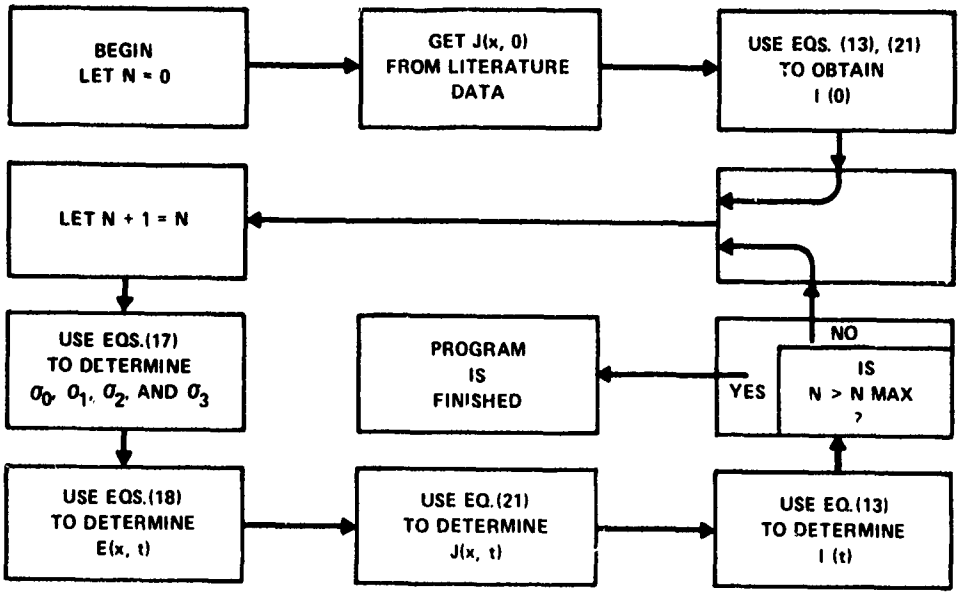

$t \equiv N\Delta t$

Eq. (13) $$I(t) = \frac{1}{a}\int_0^a J(x,t)\,dx - \frac{1}{c-b}\int_b^c J(x,t)\,dx$$

Eq. (17)
$$\begin{cases} \sigma_0(t) = \sigma_0\left(\Delta t\,(N-1)\right) + \Delta t\left[-J\left(0\ \Delta t\,(N-1)\right) + \frac{1}{a}\int_0^a J\left(x,\,(N-1)\ \Delta t\right)dx\right] \\ \sigma_1(t) = \sigma_1\left((N-1)\,\Delta t\right) + \Delta t\left[J\left(a,\Delta t\,(N-1)\right) - \frac{1}{a}\int_0^a J\left(x,\,\Delta t\,(N-1)\right)dx\right] \\ \sigma_2(t) = \sigma_2\left((N-1)\,\Delta t\right) + \Delta t\left[-J\left(b,\Delta t\,(N-1)\right) + \frac{1}{c-b}\int_b^c J\left(x,\,\Delta t\,(N-1)\right)dx\right] \\ \sigma_3(t) = \sigma_3\left((N-1)\,\Delta t\right) + \Delta t\left[J\left(c,\Delta t\,(N-1)\right) - \frac{1}{c-b}\int_b^c J\left(x,\,\Delta t\,(N-1)\right)dx\right] \\ \sigma_0(0) = \sigma_1(0) = \sigma_2(0) = \sigma_3(0) = 0 \end{cases}$$

Eq (18)
$$\begin{cases} 0 \le x \le a,\ E(x,t) = \frac{1}{\epsilon}\left[\sigma_0(t) - \sigma_1(t) + \Delta t\sum_{m=0}^{N-1}\left[J(a,m\Delta t) - 2J(x,m\Delta t) + J(0,m\Delta t)\right]\right] + E(x,0) \\ b \le x \le c;\ E(x,t) = \frac{1}{\epsilon}\left[\sigma_2(t) - \sigma_3(t) + \Delta t\sum_{m=0}^{N-1}\left[J(c,m\Delta t) - 2J(x,m\Delta t) + J(b,m\Delta t)\right]\right] + E(x,0) \end{cases}$$

Eq. (21) $$J(x,t) = J(x) + E(x,t)\left[\upsilon_0 + \upsilon_R \dot{D}(x)\right]$$

Figure 3. Computer Program Flow Chart

The analysis presented is a straightforward application of electrostatic equations to a one-dimensional linear dielectric material. Similar analyses[1] have been published for various applications (such as vacuum tubes, semi-conductors and others) and can be found in many textbooks on applied electrodynamics. We have included a derivation of the equations to make clear the exact conditions and assumptions with which we are working.

The equations are valid under the following conditions:

(a) ϵ is constant throughout the dielectric.

(b) The dielectric is in reasonable contact with the metal plates during irradiation. Radiation-induced, low-energy electron emission effectively short circuits any gaps between materials.

(c) The electron flux directly generated by the high energy radiation is not significantly perturbed by the electrostatic fields.

(d) J and E are functions of only x and t.

(e) The radiation-induced conductivity must be known and must vary slowly with E; that is, no avalanching or breaking down effects are considered.

Electron currents generated within the dielectric by the radiation create the new and peculiar twist shown by these equations. Moving electrons can originate and "die" entirely within the dielectric. Generally, the energy distribution of these electrons is such that the electric fields do not substantially alter the trajectory of the vast majority of the high energy electrons. The radiation-induced, high-energy currents J(x) can be calculated from the photoelectric, compton, and high energy electron transport effects. Radiation simultaneously excites low energy electrons which are strongly affected by the electrostatic fields.

4. DETERMINATION OF THE PHOTO-COMPTON CURRENT, J(x)

4.1 Historical Background

A historical perspective aids one in understanding the approach in this report. High energy radiation transport has been a large important field, both economically and politically, for 30 years. The major radiation interactions can be quantitatively discussed such that many engineering solutions can be deduced from physical laws. Many important economic and military problems have been heavily studied. Specifically, the design of fission reactions to optimize output, the design of

1. Marx, K.D. (1973) IEEE Trans. Nuc. Sci. NS20(No. 6):64-71. (In this paper, equations are derived for a transmission line under conditions which could be caused by radiation.) Also see Birdsall, Charles K., and Bridges, William B. (1966) Electron Dynamics of Diode Regions, Academic Press Inc., New York, N.Y.

shields to attenuate penetrating radiations from reactions, the calculation of space and atmospheric transmission of nuclear radiations, the interaction of radiations with biological tissue, the use of radiation processing to create better materials, and the displacement of atoms in solids are all problems of strong continuing interest.

A great deal of effort has produced useful quantitative information which can be quickly applied to many specific engineering problems. Most of this information involves an energy flux or an energy transport since many of the above mentioned effects can be approximately related to the radiation energy density. Nearly always, the energy transport is accompanied by a current flow of high energy electrons. It is rare that the current flow, $\vec{J}$, is responsible for tissue damage, reactor shielding problems, or atomic displacements; the energy density term correlates more strongly with these effects. But we now have computational techniques for determining the energy density for many kinds of radiation in many arrangements of matter.

From the computational techniques developed for determining the radiation energy density, we can determine the current flow $J(x)$ in some geometries. It is not a simple problem. The present state of the art is best displayed in Reference 2 and in the references contained in Reference 2. In this reference a current $J(x)$ is calculated for monoenergetic monodirectional photons in homogeneous material. $J(x)$ is tabulated for 25 elements and 10 insulating compounds under photon radiation of energies from 0.01 MeV to 20.0 MeV. However, the restriction to homogeneous materials is too severe for most applications. An example of application to a nearly homogeneous apparatus is given in Reference 3.

The situation for non-homogeneous material has been generally "ignored" by analytical workers since the problem appears to be very complex. Occasionally, apparently motivated by some application, experimentalists have made measurements of $J(x)$ at an interface between two metals.[4,5,6]

A large number of measurements under non-rigorous conditions were made of the current flowing to metal plates imbedded in a dielectric, thus attempting to use the device as a radiation detector; the exact dependence of $\vec{J}(x, y, z, t)$ was not known. For information on these metal-dielectric experiments, see Reference 7 and especially see the references listed extensively therein.

2. MacCallum, Crawford J. and Dellin, Theodore A. (1973) J. Appl. Phys. 44 (No. 4):1878-84.
3. Brumley, F. B., et al (1973) IEEE Trans. Nuc. Sci. NS-20(No. 6):48-57.
4. Hess, Bernhard (1959) Zeit. Ang. Physik. Band 11 Heft 12:449-53.
5. Raab, Bernard (1963) Nucleonics 21(No. 2):46-7.
6. Ebert, P. J. and Lauzon, A. F. (1967) Rev. Sci. Inst. 38(No. 12):1747-52.
7. Fewell, T. R. (1972) Compton Diodes: Theory and Development for Radiation Detectors, Sandia Labs, Albuquerque, N. M., Report SC-DR-720118.

Approximate analytical techniques have been devised to make rough calculations of the currents near an interface. Many works have assumed that an electron is initially generated by the photoelectric, compton, and Auger effects and then travels in a straight line until it stops one range away. Such a calculation can only give order-of-magnitude estimates for the spatial average current and can often give the wrong sign of I. Near an interface, the multiple scattering of electrons and the discontinuous change in the high energy electron generating function can actually reverse the direction of $\bar{J}(x)$ over a finite spatial interval. The equations developed earlier indicate that we need to know div $\bar{J}(x,t)$ to determine the time-dependent currents and fields in a dielectric; this requires relatively accurate knowledge of the spatial dependence of $\bar{J}(x)$.

Work is progressing at this laboratory and elsewhere[8] to measure the spatial dependence of $\bar{J}$ in planar goemetry for non-homogeneous slabs. Calculational schemes are being developed to determine $\bar{J}(x,y,z,t)$ for more complex geometry. The planar experiments will be used to test or validate the computations. When the computations properly predict the planar experiments, they may be used to determine the time-dependent current for radiation spectra and more complex geometries which are of interest to the Air Force.

4.2 Approximate Functions for J(x)

Short of having exact functions for J(x) determined by experiment and computation, we give approximate J(x) for a few geometrical cases. Similar approximations can be found described in Reference 9. In these curves we neglect the relatively small effect due to photon attenuation.

We consider 1.25 MeV gamma rays and 0.2 MeV gamma rays incident in the normal direction. The shapes presented need not be accurate since our intent is not to make exact predictions. The curve shapes are only indicative of the kinds of effects seen with gamma rays at these energies. The curves are described in Figure 4.

In Figure 4, the number z is numerically equal to the depth in the dielectric expressed in meters. It is estimated that J(x) in these functions is everywhere within 50 percent of being correct for the given γ-ray in dielectric materials with effective $Z \leq 18$ near metals with effective $Z \geq 40$. Most of the fits are within ± 20 percent of the true data over the majority of the depth.

The data in Figure 4 applies to a single metal-dielectric interface. We can obtain $\bar{J}(x)$ for the apparatus of Figure 1 by a superposition of forward and

8. Kooi, C. F. and Kusnezov, N. (1973) IEEE Trans. Nuc. Sci. NS-20(No. 6):97-104.

9. Chadsey, William L. (1973) Monte Carlo Analysis of X-Ray and γ-Ray Transition Zone Dose and Photo-Compton Current, AFCRL-TR-73-0572.

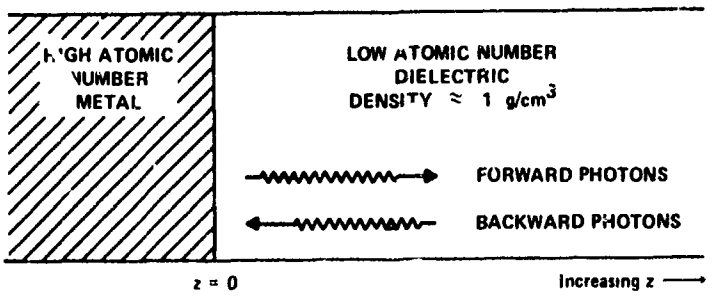

200 keV PHOTONS:

FORWARD, $J(z) \propto \left| 0.38 + \frac{1.8}{0.25 + 5.8 z^2 10^8} \right|$

BACKWARD, $J(z) \propto \left| -0.38 + \frac{1.6}{0.35 + 1.6 z^2 10^9} \right|$

600 keV PHOTONS:

FORWARD, $J(z) \propto \left| 2 + \frac{1.6}{0.4 + 6.4 z^2 10^7} \right|$

BACKWARD, $J(z) \propto \left| -2 + \frac{1.6}{0.48 + 17 z^2 10^6} \right|$

1.25 MeV PHOTONS:

FORWARD, $J(z) \propto \left| 9.4 - \frac{1.6}{0.55 + 9 z^2 10^6} \right|$

BACKWARD, $J(z) \propto \left| -9.4 + \frac{1.6}{0.25 + 4 z^2 10^6} \right|$

Figure 4. Analytical Fits to Photo-Compton Current Data

backward terms only for the case in which the dielectric and metal are each at least 1/4 electron range thick. Thinner slabs have not yet been analyzed to accurately determine the form of J(x). We will therefore always work with slabs of approximately 1 electron range thickness.

J(x) for thinner slabs is currently being experimentally determined by this author and analytically by others. The thin slab arrangement (less than one range thick) will be studied in the near future.

J(x) for other high energy radiations, such as electrons, is available but is not considered in this report.

5. RADIATION-INDUCED CONDUCTIVITY

To determine the conduction currents in the dielectric, it is necessary to know the radiation-induced conductivity everywhere in the dielectric. The high energy radiations produce a quasi-continuous energy distribution of excited electrons. The distribution extends from the valence band to the quantized energy of the incoming radiation. All of these excited electrons respond to the electric field and produce a net conductivity current. In addition, the radiation produces "holes" which can similarly respond to electric fields. The problem of determining the radiation-induced conductivity from the excited electron energy state distribution is beyond the scope of this report.

We shall take a simple empirical approach. Induced conductivity has been measured in thin insulating films under external applied bias.[10] The photoconductivity can be approximated by a linear function

$$\text{Photoconductivity} = \upsilon_R \dot{D}(x)$$

where υ_R is a constant of the material in units sec ohm^{-1} meter^{-1} rad^{-1}, and $\dot{D}(x)$ is in units rad/sec.

The data available for organic dielectrics (with dielectric constant between 1 and 10) indicates that

$$2.6 \times 10^{-17} \ \frac{\text{sec}}{\text{ohm m rad}} \leq \upsilon_R \leq 2.6 \times 10^{-14} \ \frac{\text{sec}}{\text{ohm m rad}} .$$

The value of υ_R for any one material has varied typically a factor of 10 from sample to sample and from experiment to experiment. The causes of the variance are not known. Certainly, low energy electron transport plays an important role. Experimental errors are also likely to have caused some of the discrepancies in the value of υ_R.

The work in this report does not depend on knowing υ_R accurately. We shall look at effects throughout the probable range of υ_R given above. υ_R is

10. Weingart, R. C., et al (1972) IEEE Trans. Nuc. Sci. NS19(No. 6):15-22.

an interesting factor, but it is not critical to an understanding of the qualitative features of this work. It may turn out that the experiments proposed here could be used to more accurately determine υ_R for any dielectric, but that is beyond the scope of this report.

It is essential that υ_R be effectively constant throughout any one experimental sample. Without this homogeneity all the foregoing analysis of induced conductivity is inappropriate.

6. DEPTH-DOSE DEPENDENCE, $\dot{D}(x)$

The energy deposited in matter by radiation has been extensively studied. Recent calculations and experiments have determined dose vs depth for monodirectional radiation normal to a planar interface of two materials.[11] The dose rate $\dot{D}(x)$ given in this report is obtained directly or by analogy from published and unpublished works of other people. References are given where appropriate.

By varying the spectra of incident radiation, we can vary the dose profile substantially. The dose profile may have a strong effect on the current flow in the apparatus of Figure 1. We shall hypothesize dose profiles which may or may not be possible in order to determine whether any unexpected effects are likely. It has already been shown that the dose can vary a factor of 30 or more with low energy X-rays at a high Z - low Z interface over a distance short relative to one radiation attenuation length. In principle, by mixing low energy (≤ 100 keV) X-rays with high energy (≥ 1 MeV) X-rays, it is possible to have strongly varying dose profiles and weakly varying photo-compton current J(x) profiles.

7. RESULTS

We have determined I(t), $\bar{E}(x,t)$, and $\bar{J}(x,t)$ for several material arrangements. The radiation-induced conductivity coefficient, υ_R, has been assumed to be 10^{-16} sec/ohm m rad, since this appears to be near the center of the range of

---

11. The references to this work are rather diffuse. One current starting point for information is:
Chadsey, William L. (1973) Monte Carlo Analysis of X-Ray and γ-Ray Transition Zone Dose and Photo-Compton Current, AFCRL-TR-73-0572, especially Refs. 1-4, 7, 8, 19.
Another nonoverlapping source is:
Eisen, H., Rosenstein, M., and Silverman, J. (1972) Radiation Research 52: 429.
And another is:
Dutreix, J. and Bernard, M. (1968) Biophysik 4:302.
The radiation shielding community has extensive dose depth data for homogeneous materials, and the radiation therapy field has studied skin-air, and tissue-bone interface profiles.

probable values for organic dielectrics. The permittivity is assumed to be $\epsilon = 2 \times 10^{-11}$ F/m. The external voltage is zero in all cases.

7.1 Entirely Homogeneous Material

Let the metal and dielectric materials be of the same effective atomic number. The photo-compton current profile, J(x), can be obtained as follows:

(1) Determine the photon number angle energy spectra vs depth in the material from the literature on X-ray and γ-ray attenuation and shielding.

(2) Determine the resulting depth dependent photo-compton current using, say, Ref. 2.

The dose-depth dependence can also be obtained from the extensive literature on radiation shielding. For the homogeneous case of dimensions given below, a simple exponential dependence,

$$J(x) = J(0)e^{-\mu x}$$
$$\dot{D}(x) = \dot{D}(0)e^{-\mu x}$$

is approximately correct. The approximation is sufficient for the purpose of this report. The attenuation coefficient, μ, is given in meters^{-1} and varies strongly with photon energy.

The results are given in Figures 5 and 6.

Figure 5: 1.25 MeV photons, 10^{14} photons/m^2-sec on ethylene.

$$\dot{D}(0) = 5 \text{ rad/sec}$$
$$J(0) = -1.3 \times 10^{-7} \text{ A/m}^2$$
$$\mu = 6 \text{ m}^{-1}.$$

E(x,t) and J(x,t) are graphed in Figure 5 at t = 0, $t = 10^4$, and $t \geq 10^5$ sec. The net current to the meter, $I(t) = -7.4576 \times 10^{-9}$ at $t \geq 10^5$, and $I(t = 0) = -7.4582 \times 10^{-9}$ A/m^2. There is very little time dependence in the meter current.

Figure 6: 0.2 MeV photons, 10^{14} photons/m^2-sec on ethylene.

$$\dot{D}(0) = 1 \text{ rad/sec}$$
$$J(0) = -4.5 \times 10^{-9} \text{ A/m}^2$$
$$\mu = 14 \text{ m}^{-1}.$$

The net current to the meter, I(t), varies little with time: $I(t = 0) = -.499787 \times 10^{-10}$ A/m^2 and $I(t \geq 10^6) = -.499786 \times 10^{-10}$ A/m^2.

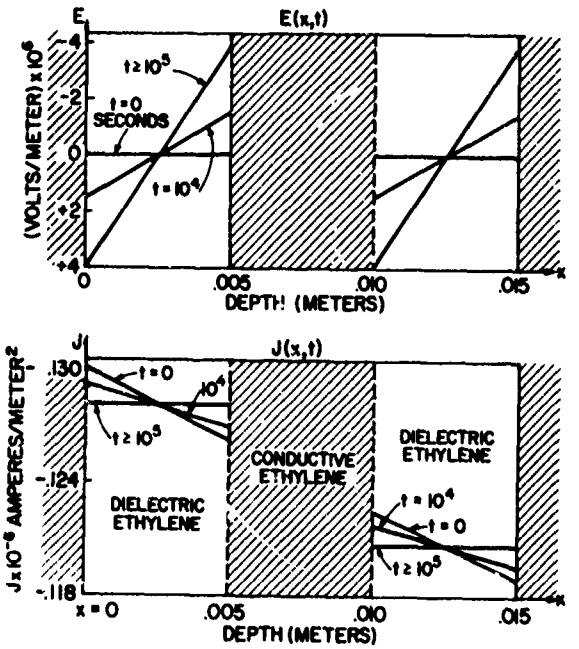

Figure 5. 1.25 MeV Photons on Homogeneous Ethylene, 10^{14} Photons/m^2-sec

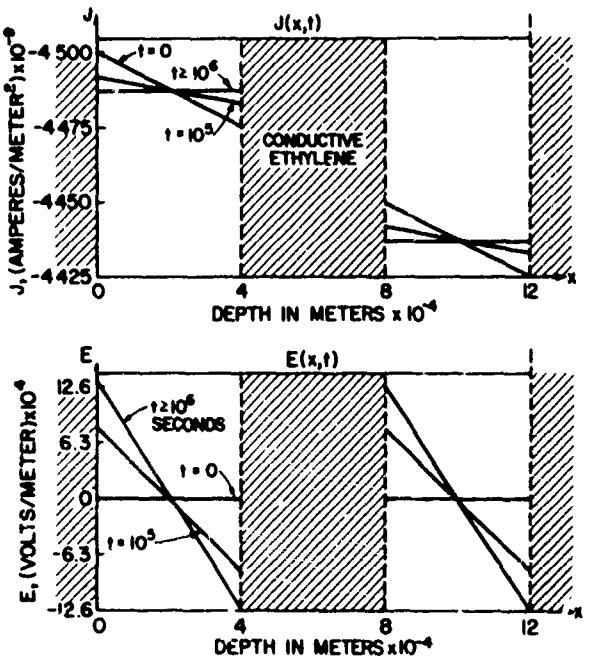

Figure 6. 0.2 MeV Photons on Homogeneous Ethylene, 10^{14} Photons/m^2-sec

Since the material is homogeneous, there are no steep curves for $\dot{D}(x)$ or $J(x)$ and the data is relatively simple. These graphs are included so that comparison of magnitudes may be made between the homogeneous and non-homogeneous case. Homogeneous materials of effective atomic number different than ethylene give qualitatively similar results.

We next consider situations where $\dot{D}(x)$ and $J(x)$ are strongly varying functions.

7.2 Center Electrode of Differing Atomic Number

Consider the apparatus of Figure 7. We can vary Z_1 and Z_2 to obtain different effects. As always, the grounded elements must be good conductors and the remaining two elements are dielectrics.

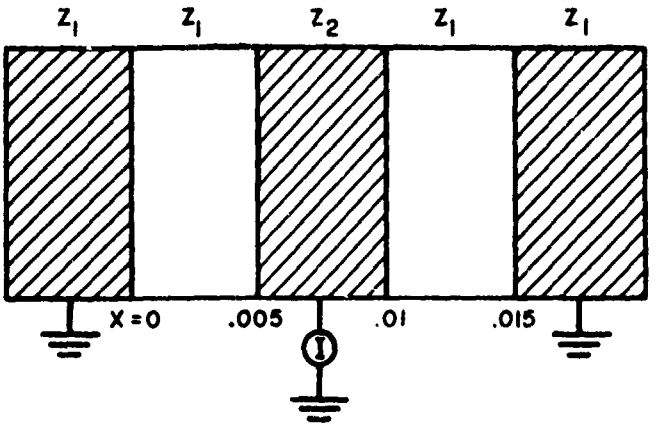

Figure 7. Apparatus With Center Electrode of Differing Atomic Number, Z

(1) $Z_2 >> Z_1$

(a) 10^{14} photons/m^2-sec, 1.25 MeV, at $x = 0$, moving in positive x direction. $Z_1 \simeq 5$ and $Z_2 \simeq 29$ so that the materials are similar to ethylene and copper. Let Z_1 have a density, $\rho \simeq 1.0$ g/cm^3 and a dielectric constant $\epsilon = 2 \times 10^{-11}$ F/m.

The functional fits for $J(x)$ and $\dot{D}(x)$ are:

$$0 \le X \le a; \quad J(x) = \left[-9.4 + 1.6 \Big/ \left(0.25 + 0.55\,(0.005 - x)^2\, 10^6\right)\right] 1.4 * 10^{-8} \frac{\text{amp}}{m^2}$$

$$b \le x \le c; \quad J(x) = \left[-9.4 + 1.6 \Big/ \left(0.55 + (1.1x - .011)^2\, 10^6\right)\right] \quad 1.3 * 10^{-8} \frac{\text{amp}}{m^2}$$

$$0 \le x \le a; \quad \dot{D}(x) = 5\left[1 + 1\Big/\left(1 + (0.005 - x)^2 * 4 * 10^5\right)\right] \frac{\text{rad}}{\text{sec}}$$

$$b \le x \le c; \quad \dot{D}(x) = 4.8\left[1 - 0.3\Big/\left(1 + (x - 0.01)^2 * 3 * 10^5\right)\right] \frac{\text{rad}}{\text{sec}} .$$

The curve fits to dose depth are taken from the data of Ref. 12 with modification. The dose data of Ref. 12 near depth x = b (just downstream from the high Z material) contains a region of negative slope. It is assumed that this region of Ref. 12 data is due to low energy photons ($\le$400 keV) causing electron photoemission from the high Z into the low Z material. This low energy photoemission component of the dose has been subtracted out to obtain dose due to 1.25 MeV photons alone. Monte Carlo calculations of dose near an interface strongly support this subtraction of the alleged low energy component.[13] The dose depth curves of Ref. 13 are also similar to the fits given above.

The results for $Z_2 >> Z_1$ are shown in Figure 8. Two especially interesting results obtain:

1) the electric fields approach 10^8 V/m which could cause dielectric breakdown in some materials, and
2) the meter current begins positive and then becomes negative as the exposure progresses in time.

(b) 200 keV photons, 10^{14} photons/m^2-sec incident in positive direction at x = 0. The approximate fits to the available data[13] for J(x) and $\dot{D}(x)$ can be seen in Figure 9. Note that J(x) = J(x, 0).

The resulting I(t), J(x,t), E(x,t) are plotted in Figure 9. The most interesting features are:

1) The maximum electric fields are again approximately 10^8 V/m;
2) The meter current, I, changes a factor of 4 with time;
3) The final equilibrium meter current is positive, not negative, as seen in the previous cases.

(2) $Z_1 >> Z_2$

Let the metal electrode be beryllium or carbon, and let the dielectric material have a relatively high effective Z such as Saran or polyvinyl-chloride or SiO_2 or Al_2O_3. Dielectrics with higher effective Z can be found such as tantalum oxide, but we have not considered these.

(a) 200 keV photons incident on PVC dielectric with beryllium center electrode. 10^{14} photons/m^2-sec are incident at x = 0. The curve fits to the available data are not to be taken as true curve fits. The available data is not complete but is "good enough" to give us approximately correct fits. Therefore,

12. Frederickson, A. R. and Burke, E. A. (1971) IEEE Transactions on Nuclear Science NS18:162-9.

13. Long, David M., Chadsey, William L., and Benedict, Robert V. (1971) Prediction of Dose Gradients and Their Effects on Semiconductors, AFCRL-71-0584.

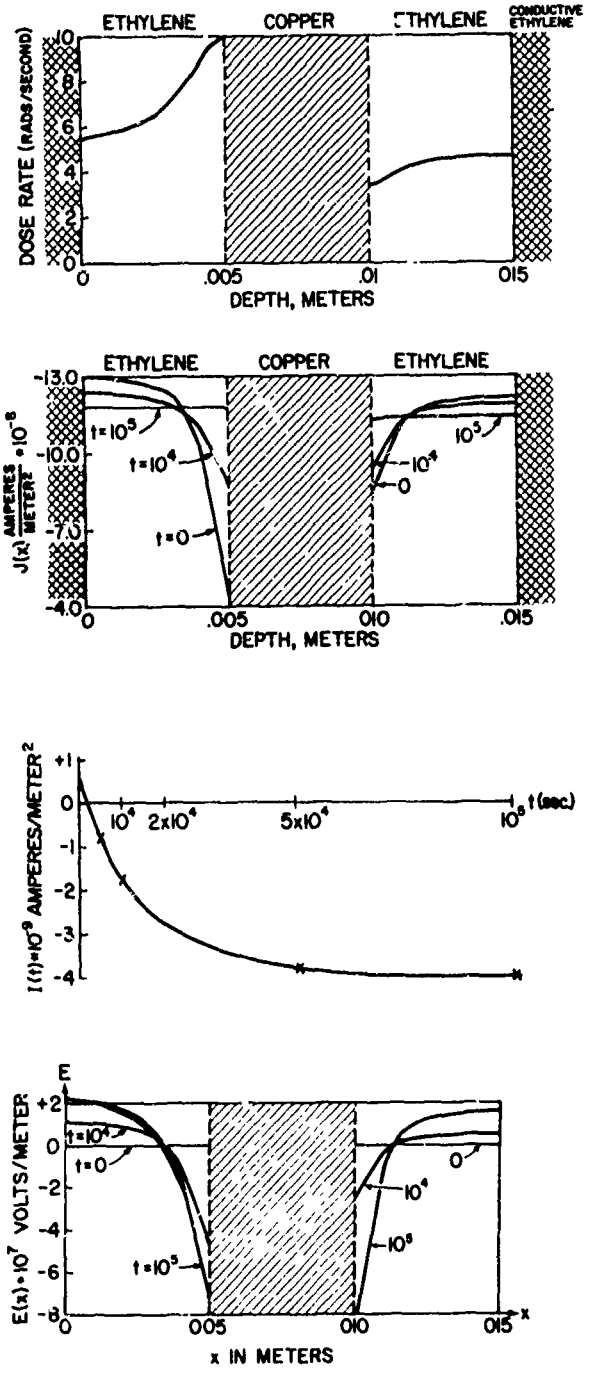

Figure 8. 1.25 MeV Photons, 10^{14} Photons/m^2 -sec on Ethylene With High Z Center Electrode

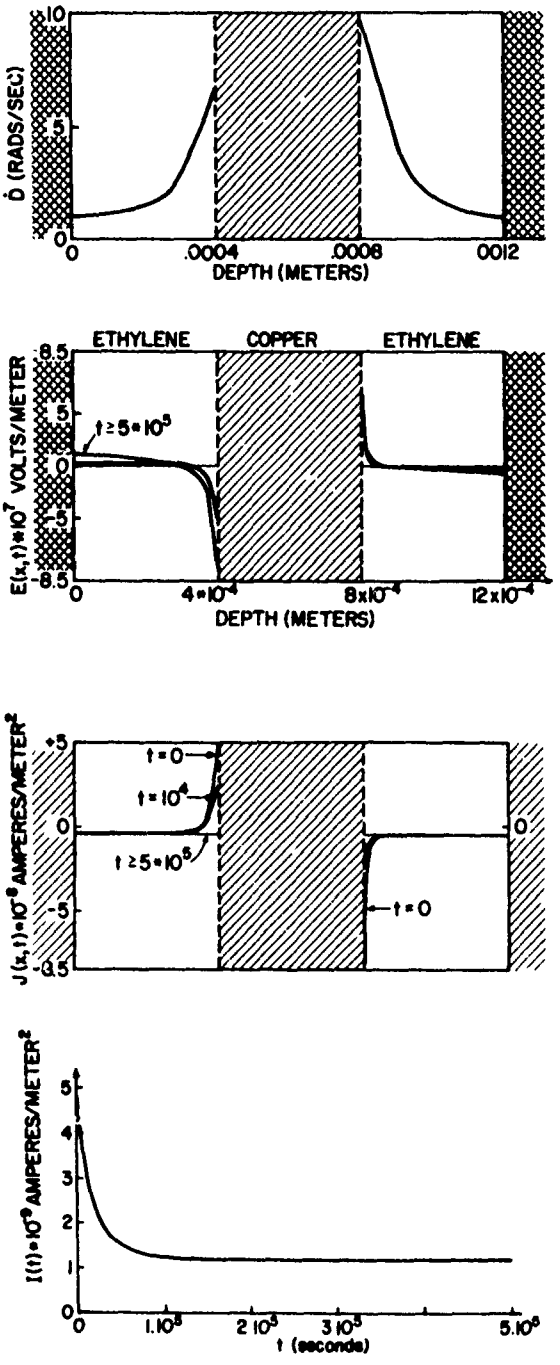

Figure 9. 200 keV Photons, 10^{14} Photons/m^2-sec on Ethylene With High Z Center Electrode

the results for J(x,t), E(x,t), and I(t) are only indicative of the effects to be seen. Exact predictions for 200 keV photon beams cannot be made at this time due to the lack of accurate interface photo-compton current and interface dose data with this material combination. Results are shown in Figure 10.

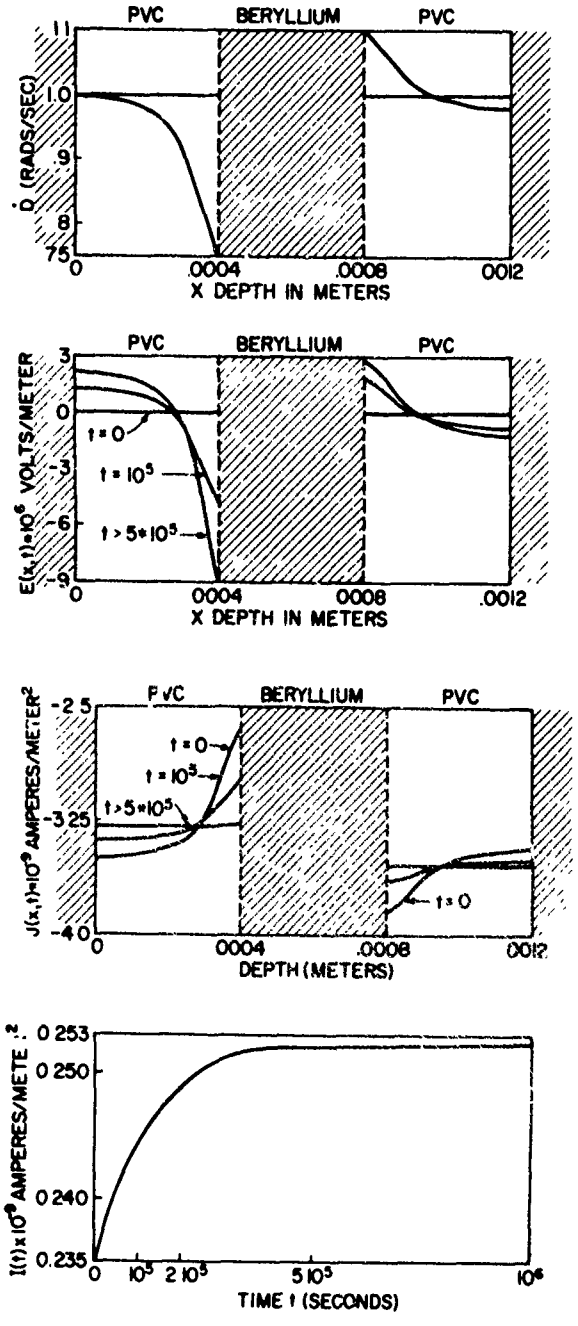

Figure 10. 0.2 MeV Photons, 10^{14} Photons/m^2 -sec on PVC With Beryllium Center Electrode

In this case, I(t) changes about 8 percent and the electric fields peak at $\sim 10^7$ V/m. These effects are significantly reduced compared to Figure 9. In general, the effects can be expected to be a minimum as the materials approach each other in atomic number. Strong effects could still be seen for low Z - low Z materials if the photon energy were below 20 keV. We do not have adequate dose-depth data and photo-compton current data at the lower energies to do the proper analysis.

(b) 1.25 MeV photons would produce effects qualitatively the same as the 200 keV photons. We will not include results for the 1.25 MeV photons for this geometry.

7.3 Outer Electrodes of Differing Atomic Number

(1) $Z_1 >> Z_2$ as shown in Figure 11.

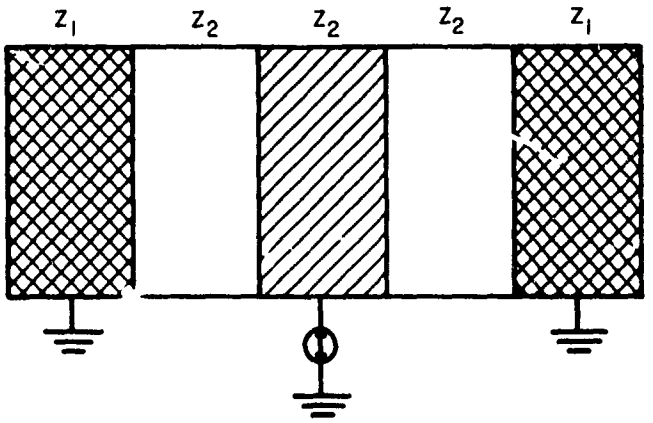

Figure 11. Apparatus With Outer Electrodes of Different Material

(a) 1.25 MeV photons on, say, $Z_1 = 29$ and $Z_2 \simeq 5$ (ethylene). We can obtain $\dot{D}(x)$ and $J(x)$ caused by 10^{14} photons/m^2-sec at $x = 0$. Again the dielectric density is $\simeq 1.0$ g/cm^3. The results, shown below in Figure 12, indicate that I(t) varies less than in Figure 8. This probably is due to the mutual cancellation of opposing effects in the two dielectrics. The maximum E(x,t) is analogous to Figure 8 and occurs near the outer electrodes.

(b) 200 keV photons, 10^{14} photons/m^2-sec incident on $Z_1 = 29$ and $Z_2 \simeq 5$ (ethylene). The resulting J(x,t), E(x,t), $\dot{D}(x)$, and I(t) are given in Figure 13. The results show again that the time dependent fields and currents

produce a time dependent meter current I(t), and that peak electric fields of nearly 10^3 V/m can be reached.

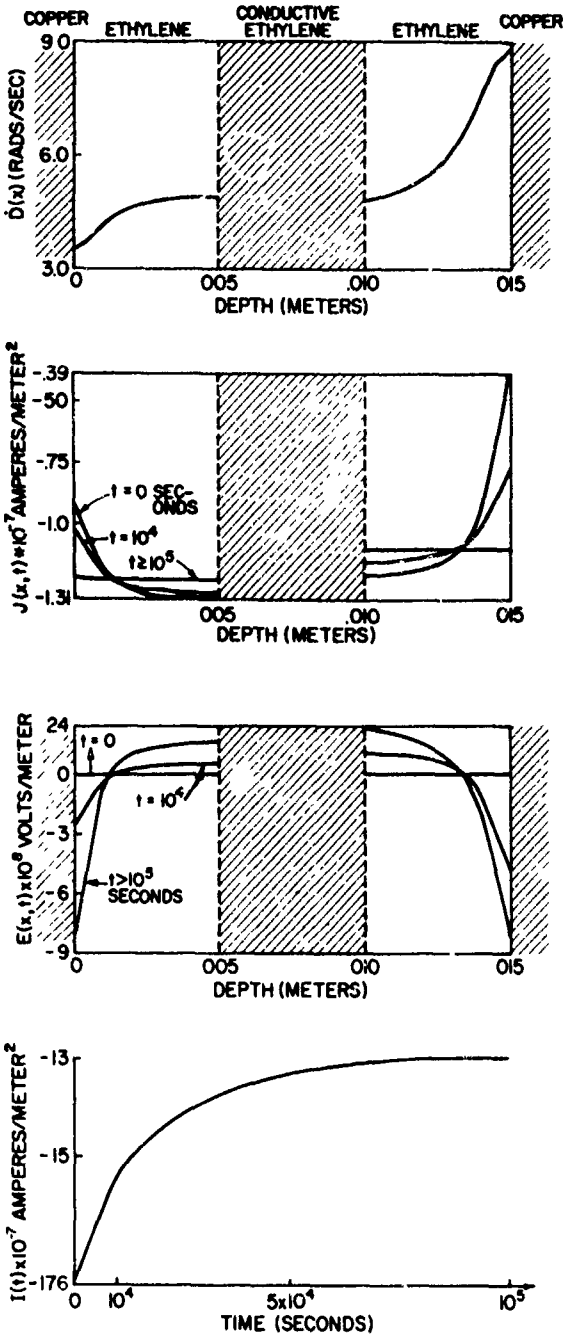

Figure 12. 1.25 MeV Photons, 10^{14} Photons/m^2 -sec on Copper Surrounding Ethylene

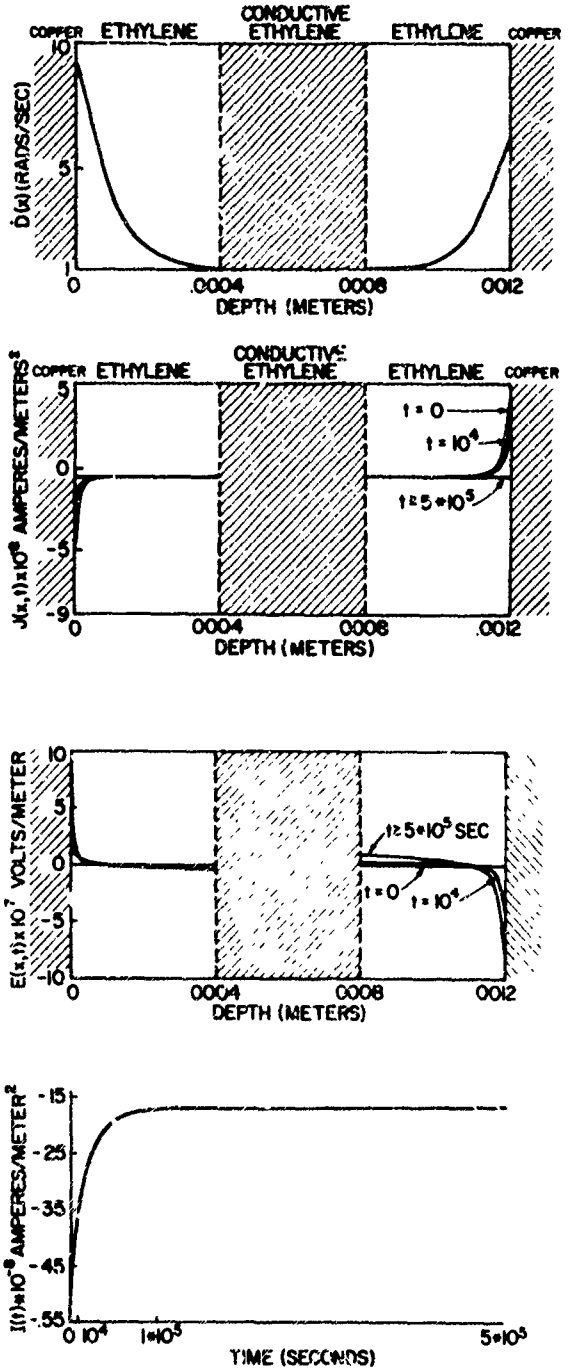

Figure 15. 200 keV Photons, 10^{14} Photons/m^2 -sec on Copper Surrounding Ethylene

7.4 Further Cases

It is possible to permute the material atomic numbers in several additional ways. For example, we might enhance the maximum electric field by the following structure:

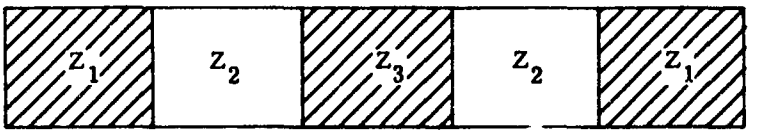

$$Z_1 \ll Z_2 \ll Z_3$$

It has been shown[12] that this type of material combination produces greater dose gradients and a greater divergence of photo-compton currents than the cases already discussed. The increased dose gradients and current divergence will usually result in increased electric fields and significantly differing meter currents, I(t). However, it is not qualitatively instructive to make more permutations, so we have not done so here.

7.5 Mixed Photon Spectra

Interesting cases might occur when several photon energies are simultaneously applied. The only mixed spectra case we have considered to date is similar to Sec. 7.2(1), but with both 200 keV and 1250 keV photons of equal number intensity. Many other spectra combinations might be of interest but they will not be considered here.

In this case we have a high Z center electrode surrounded by low Z dielectrics and low Z outer electrodes. The total dose rate and the total photo-compton current are each the sum of the 200 keV and 1250 keV dose rate and photo-compton currents respectively. For the sake of variety, we have changed the radiation-induced conductivity constant, $\mathcal{O}_R$ to $\mathcal{O}_R = 10^{-15}$ sec/ohm-m-rad. (In previous examples, $\mathcal{O}_R = 10^{-16}$.) If we compare the results with Sec. 7.2, we see that the time-to-reach-equilibrium and the electric field strength are a factor 10 lower in these latest results due to the change in $\mathcal{O}_R$ value. The results are shown in Figure 14.

Overall, the results are fairly similar to Sec. 7.2; however, one interesting result stands out. Notice that the electric field changes sign twice as we vary depth in the right dielectric. There are two depths in the dielectric at which the electric field becomes zero. In all previous cases, there is only one depth at which the electric field is zero. If we look at the plot of J(x, 0) and consider its

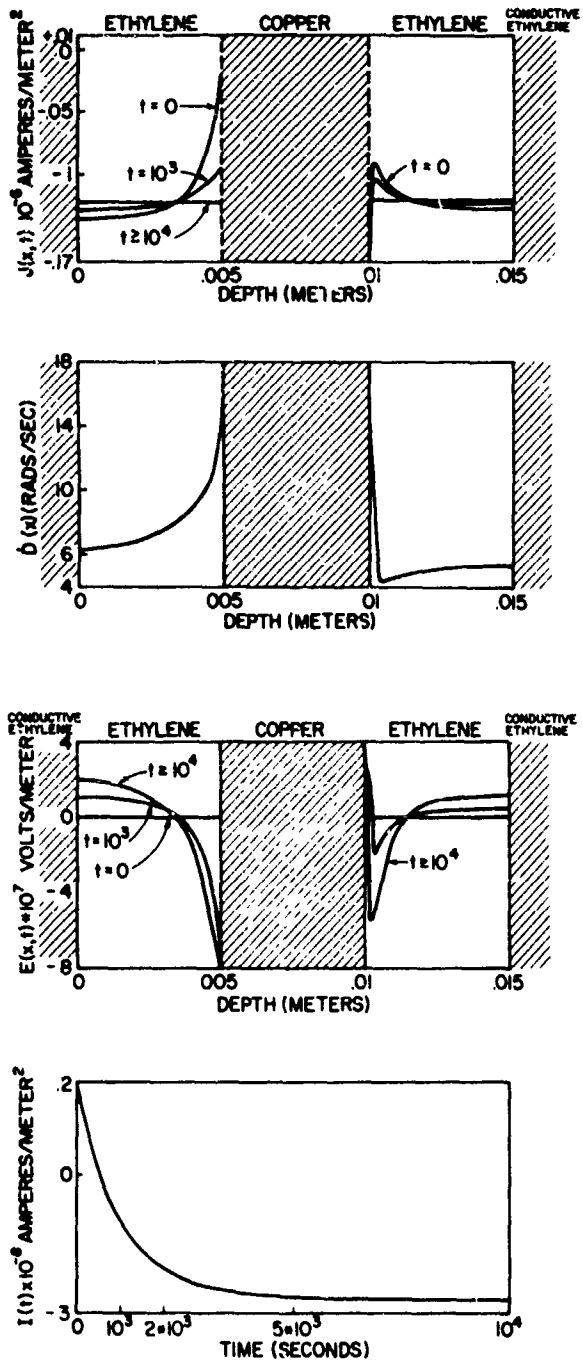

Figure 14. Results for a Mixed Spectra, 10^{14} Photons/m^2-sec at 1250 keV and at 200 keV on Ethylene Surrounding Copper

divergence we see that alternate layers of positive and negative charge are being deposited in the dielectric at various depths. If we were to change the right conductor to a high Z material, the photo-compton current would produce a third depth at which the electric field is zero. Furthermore, by adding layers of differing Z dielectric and by irradiating from non-normal directions, we might find it possible to increase the number of electric field nodal points indefinitely.

If the dielectric layers were relatively thin, it might be that the low energy components of a mixed spectrum would produce the predominant effects. For example, suppose we have a field effect transistor with a $\lesssim 10^4$ Å dielectric. Assume a fluence with a continuous spectrum from 1 MeV to 0 eV. The electrons above 100 keV would be virtually unperturbed by the interface. Lower energy electrons would be more strongly affected by the dielectric metal interface. The abrupt change in electron scattering properties at the metal dielectric interface could affect lower energy electric transport most strongly. Also, the abrupt change in photoelectric cross section would cause highly diverging photoelectron currents for photons below 100 keV. The net result is that for thin dielectrics, the total charge deposition may depend most heavily on the low energy components of the radiation fluence. The effects of mixed spectra on thin dielectrics presents a whole new array of possibilities.

7.6 Dependence on υ_R

Earlier we noted that the radiation induced conductivity coefficient, υ_R, is not accurately determined. It is possible to obtain the functional dependence of $E(x,t)$, $I(t)$, and $J(x,t)$ on υ_R from the equations given earlier, but we have not done so. Instead, we have used the data of Sec. 7.2 with several values of υ_R to determine the effect of varying υ_R. In this way, our data can be extrapolated for other values of υ_R. It turns out that if we have calculations of $J_0(x,t)$, $E_0(x,t)$, and $I_0(t)$ for a specific value of υ_R, say $\upsilon_R = \upsilon_{R0}$, then we can determine $J(x,t)$, $I(t)$, and $E(x,t)$ for any value of υ_R as follows:

$$J(x,t;\upsilon_R) = J_0\left(x, \frac{\upsilon_R}{\upsilon_{R0}}t\right)$$

$$E(x,t;\upsilon_R) = \frac{\upsilon_{R0}}{\upsilon_R} E_0\left(x, \frac{\upsilon_R}{\upsilon_{R0}}t\right)$$

$$I(t;\upsilon_R) = I_0\left(\frac{\upsilon_R}{\upsilon_{R0}}t\right).$$

These relationships are valid only when $\upsilon_R \dot{D} \gg \upsilon_0$. Notice that the changes in υ_R produce simple transformations of the time and electric field intensity axis. There is no change in the spatial dependence for E or J and the initial and final values for I and J are unchanged.

The physical explanation for the υ_R dependence is simple. The initial photo-compton current, J(x), is fixed by the geometry independent of υ_R. The resulting spatial charge deposition produces electric fields which increase with time until DIV J = 0 and no more charge is deposited. The electric field simply builds up to the level required to produce the conduction currents necessary to create a J such that DIV J = 0. A change in υ_R does not change the spatial dependence of either the charge deposition or the conduction currents, but only changes the intensity of the conduction currents for a given E. Thus, if we decrease υ_R, the system reacts by letting the initial charge deposition continue longer, until E is finally increased sufficiently to cause the necessary equilibrium conduction currents. Thus the spatial dependence of J(x,t) is unaffected. Only the time to reach equilibrium, and the final electric fields are affected by changing υ_R.

8. APPLICATION TO ELECTRONIC DEVICES

In addition to the FET discussed above, coaxial cables, dielectric compton diodes, capacitors, and LSI circuits are all directly affected by charge injection effects. Time-dependent currents to conductors have been seen in coaxial cables[14] and dielectric metal sandwiches.[15] LSI and MOS devices exhibit trapped charge in the dielectrics under irradiation, and the trapped charge distribution is often dependent on an applied electric field. The mechanism discussed in this paper may play an important role in these devices.

Our ability to apply this mechanism to actual three-dimensional devices is presently limited. It is very difficult to calculate the photo-compton currents at a one-dimensional interface. Two-dimensional interfaces have not yet been done to our knowledge, but the potential exists; it is only required that a Monte Carlo program be developed for a representative geometry, such as a coaxial capacitor geometry. For cases with thin dielectric layers, a computer program must be especially dedicated to determining the currents and charge depositions in that layer. However, the currents in the dielectric layer depend on the electron scattering histories in material outside the layer. It seems to us that the thin dielectric problem will require computer programs especially dedicated to this one

14. van Lint, V. A. J. (1970) IEEE Trans. Nuc. Sci. NS17:210-16.

15. Sullivan, W. H. and Ewing, R. L. (1971) IEEE Trans. Nuc. Sci. NS18:313 (Fig. 5).

geometry so that we maintain the spatial detail so necessary for calculations inside the dielectric.

Let us look at a thin layer problem. Unpublished in-house data for 100 Roentgen-cm^2/sec cobalt 60 photon beam on a low Z - high Z interface deposits charge in the first 10^5 Å of low Z material at the rate of 2×10^{-13} C/cm^2-R. If we do a linear extrapolation in depth, then a 10^3 Å layer receives charge at the rate of 2×10^{-15} C/cm^2-R. For a total fluence of 10^6 R (cobalt 60), we get a charge deposition of 2×10^{-9} C/cm^2. Such a surface charge density on a layer of SiO_2 of 10^3 Å thickness produces a voltage of ~0.1 V. If the layer were 10^4 Å thick, then the voltage developed would be 10 V. To calculate the charge deposition in a 10^3 Å layer requires doing better than a linear extrapolation in thickness, since the plot of charge deposition vs depth has a steep slope for thickness less than 10^5 Å. We are currently unable to make a correct extrapolation to 10^3 Å thickness but we hope to be able to do so in the future. The charge buildup in the irradiated ~10^3 Å gate dielectric of MOS devices may be affected by the mechanism given in this report. To this author's knowledge, this mechanism has not been given consideration.

The unstable response of dielectric compton diodes might be explained by this general model. However, the compton diode geometry generally in use would require a difficult three-dimensional, coupled electron-photon transport code. The planar slab compton diode is probably solvable with currently available data. The vacuum compton diode avoids the dielectric charging difficulty but has less sensitivity. The multiple high Z - low Z slab vacuum compton diode* gives factor of ten sensitivity gain without the dielectric problem but appears to be limited to slab geometry and collimated beams.

Radiation-induced conductivity coefficients have been determined by irradiating dielectric slabs between biased metal plates and measuring the bias current. We have shown here that tremendous electric fields are built-up internal to the dielectric. Therefore the data taken with biased metal plates may be incorrect since the internal electric field strength was not correctly measured. It may be more accurate to use a dielectric slab in the geometry of Figure 1 with a known J(x) profile to determine the induced conductivity from the measured time dependence of I(t).

---

*Also see U.S. Patent No. 3, 780, 304, Charge Accumulation Gamma Radiation Detector.

9. CONCLUSIONS

A method has been developed for determining the time-dependent currents and electric fields in a dielectric-metal structure in one-dimensional slab geometry. Results are given for 200 keV and 1250 keV photon irradiation on typical materials. Interesting results include time-dependent electrode currents which reverse sign, and electric fields which reach 10^8 V/m.

We have shown that the dose depth dependence and electron current depth dependence strongly affect the currents to metal elements (sometimes called replacement currents). An electric field builds up with time, producing a time-dependent conduction current. When equilibrium is reached, the high energy electron current and the conduction current sum to a net current whose divergence is everywhere zero. This net current can be very different from the "no field" currents normally used to predict "replacement currents" in irradiated devices.

The relaxation time predicted here for organic dielectrics is virtually identical to the measured relaxation time reported for dielectrics in MOS-FET devices. Furthermore, this relaxation time could be the basis for time-dependent effects seen in irradiated capacitors.

At this time it appears prudent to experimentally check the results presented here. If the calculations are experimentally confirmed, then it would be of interest to obtain the information necessary to quantitatively predict the response of some devices. This prediction might show, for example, that capacitor responses will always be time dependent and radiation history dependent. It might also show that MOS devices will always have dielectric charging, but that the charging can be minimized by a judicious choice of surrounding material. To predict such device response, we require information on $\bar{J}(x)$ and $\dot{D}(x)$ in the appropriate geometry. This information is currently lacking.

References

1. Marx, K. D. (1973) IEEE Trans. Nuc. Sci. NS20(No. 6):64-71. (In this paper, equations are derived for a transmission line under conditions which could be caused by radiation.) Also see Birdsall, Charles K., and Bridges, William B. (1966) Electron Dynamics of Diode Regions, Academic Press Inc., New York, N.Y.
2. MacCallum, Crawford J. and Dellin, Theodore A. (1973) J. Appl. Phys. 44 (No. 4):1878-84.
3. Brumley, F. B., et al (1973) IEEE Trans. Nuc. Sci. NS-20(No. 6):48-57.
4. Hess, Bernhard (1959) Zeit. Ang. Physik, Band 11 Heft 12:449-53.
5. Raab, Bernard (1963) Nucleonics 21(No. 2):46-7.
6. Ebert, P. J. and Lauron, A. F. (1967) Rev. Sci. Inst. 38(No. 12):1747-52.
7. Fewell, T. R. (1972) Compton Diodes: Theory and Development for Radiation Detectors, Sandia Labs, Albuquerque, N. M., Report SC-DR-720118.
8. Kooi, C. F. and Kusnezov, N. (1973) IEEE Trans. Nuc. Sci. NS-20(No. 6):97-104.
9. Chadsey, William L. (1973) Monte Carlo Analysis of X-Ray and γ-Ray Transition Zone Dose and Photo-Compton Current, AFCRL-TR-73-0572.
10. Weingart, R. C., et al (1972) IEEE Trans. Nuc. Sci. NS19(No. 6):15-22.
11. The references to this work are rather diffuse. One current starting point for information is:
    Chadsey, William L. (1973) Monte Carlo Analysis of X-Ray and γ-Ray Transition Zone Dose and Photo-Compton Current, AFCRL-TR-73-0572, especially Refs. 1-4, 7, 8, 19.
    Another nonoverlapping source is:
    Eisen, H., Rosenstein, M., and Silverman, J. (1972) Radiation Research 52: 429.
    And another is:
    Dutreix, J. and Bernard, M. (1968) Biophysik 4:302.
    The radiation shielding community has extensive dose depth data for homogeneous materials, and the radiation therapy field has studied skin-air, and tissue-bone interface profiles.

12. Frederickson, A. R. and Burke, E. A. (1971) IEEE Transactions on Nuclear Science NS18:162-3.

13. Long, David M., Chadsey, William L., and Benedict, Robert V. (1971) Prediction of Dose Gradients and Their Effects on Semiconductors, AFCRL-71-0584.

14. van Lint, V. A. J. (1970) IEEE Trans. Nuc. Sci. NS17:210-216.

15. Sullivan, W. H. and Ewing, R. L. (1971) IEEE Trans. Nuc. Sci. NS18:313 (Fig. 5).

Glossary

V	voltage in units of volts.
σ	surface charge density in units of coulombs/meter^2.
I	meter current in units of amperes/meter^2.
J	current density in units of amperes/meter^2.
ρ	volume charge density in units of coulombs/meter^3.
E	electric field intensity in units of volts/meter.
ϵ	permittivity in units of farads/meter.
A	amperes.
υ_0	conductivity in units of ohm^{-1} meter^{-1}.
υ_R	coefficient of radiation induced conductivity in units of seconds/ohm-meter-rad.
$\dot{D}$	radiation energy deposition rate in units of rads/second. (One rad = 100 erg/gram).